

HIGH STRAIN RATE MECHANICAL PROPERTIES OF EPOXY AND EPOXY-BASED PARTICULATE COMPOSITES

Jennifer L. Jordan
D. Wayne Richards
Air Force Research Laboratory
Munitions Directorate
AFRL/MNME
Eglin AFB, FL 32542-6810



Brad White
Naresh N. Thadhani
School of Materials Science and Engineering
Georgia Institute of Technology
Atlanta, GA 30332

Jonathan E. Spowart
Air Force Research Laboratory
Materials and Manufacturing Directorate
AFRL/MLLMD
Wright Patterson AFB, OH 45433

AUGUST 2007

CONFERENCE PAPER AND BRIEFING CHARTS

This paper and corresponding briefing charts were presented at the 2007 SEM Annual Conference and Exposition on Experimental and Applied Mechanics, Springfield, MA, 3-6 June, 2007. They will be published in the unclassified/unlimited distribution proceedings. One or more of the authors is a U.S. Government employee working within the scope of his/her position; therefore, the U.S. Government is joint owner of the work. When published, the Society for Experimental Mechanics may assert copyright. If so, the U.S. Government has the right to copy, distribute, and use the work by or on behalf of the U.S. Government. Any other form of use is subject to copyright restrictions.

This paper is published in the interest of the scientific and technical information exchange. Publication of this paper does not constitute approval or disapproval of the ideas or findings.

DISTRIBUTION A: Approved for public release; distribution unlimited. Approval Confirmation:
for the abstract - AAC/PA # 09-22-06-444, dated 22 September 2006 and
for the paper - AAC/PA# 03-07-07-154, dated 7 March 2007 and
for the briefing charts - AAC/PA# 05-21-07-421, dated 21 May 2007 and
AAC/PA# 11-22-06-535, dated 22 November 2006.

AIR FORCE RESEARCH LABORATORY, MUNITIONS DIRECTORATE

■ Air Force Materiel Command ■ United States Air Force ■ Eglin Air Force Base

REPORT DOCUMENTATION PAGE					<i>Form Approved OMB No. 0704-0188</i>	
<small>The public reporting burden for this collection of information is estimated to average 1 hour per response, including the time for reviewing instructions, searching existing data sources, gathering and maintaining the data needed, and completing and reviewing the collection of information. Send comments regarding this burden estimate or any other aspect of this collection of information, including suggestions for reducing the burden, to Department of Defense, Washington Headquarters Services, Directorate for Information Operations and Reports (0704-0188), 1215 Jefferson Davis Highway, Suite 1204, Arlington, VA 22202-4302. Respondents should be aware that notwithstanding any other provision of law, no person shall be subject to any penalty for failing to comply with a collection of information if it does not display a currently valid OMB control number.</small>						
PLEASE DO NOT RETURN YOUR FORM TO THE ABOVE ADDRESS.						
1. REPORT DATE (DD-MM-YYYY)		2. REPORT TYPE			3. DATES COVERED (From - To)	
4. TITLE AND SUBTITLE				5a. CONTRACT NUMBER		
				5b. GRANT NUMBER		
				5c. PROGRAM ELEMENT NUMBER		
6. AUTHOR(S)				5d. PROJECT NUMBER		
				5e. TASK NUMBER		
				5f. WORK UNIT NUMBER		
7. PERFORMING ORGANIZATION NAME(S) AND ADDRESS(ES)					8. PERFORMING ORGANIZATION REPORT NUMBER	
9. SPONSORING/MONITORING AGENCY NAME(S) AND ADDRESS(ES)					10. SPONSOR/MONITOR'S ACRONYM(S)	
					11. SPONSOR/MONITOR'S REPORT NUMBER(S)	
12. DISTRIBUTION/AVAILABILITY STATEMENT						
13. SUPPLEMENTARY NOTES						
14. ABSTRACT						
15. SUBJECT TERMS						
16. SECURITY CLASSIFICATION OF:			17. LIMITATION OF ABSTRACT	18. NUMBER OF PAGES	19a. NAME OF RESPONSIBLE PERSON	
a. REPORT	b. ABSTRACT	c. THIS PAGE			19b. TELEPHONE NUMBER (Include area code)	

High Strain Rate Mechanical Properties of Epoxy and Epoxy-Based Particulate Composites

Jennifer L. Jordan¹, Brad White², Jonathan E. Spowart³, D. Wayne Richards¹, Naresh N. Thadhani²

¹ Air Force Research Laboratory, Munitions Directorate, AFRL/MNME, Eglin AFB, FL 32542

² School of Materials Science and Engineering, Georgia Institute of Technology, Atlanta, GA 30332

³ Air Force Research Laboratory, Materials and Manufacturing Directorate, AFRL/MLLMD, Wright-Patterson AFB, OH 45433

ABSTRACT

Polymers and polymer-based particulate composites are becoming increasingly used in aerospace structural applications, where they experience complex, non-static loads. Correspondingly, the high strain rate mechanical properties are of increasing importance. This paper investigates the properties of epoxy - bisphenol-A/diethanolamine epoxy (Epon 826/DEA) – and epoxy-based particulate composites across strain rates from 10^{-3} to 10^5 /s. The samples were tested using Instron, traditional split Hopkinson pressure bars (SHPBs) and a miniaturized SHPB for ultra-high strain rates. Additionally, the epoxy samples are tested with dynamic mechanical analysis to look at the effects of time-temperature superposition on the strain rate effects in the samples. The results of the testing are compared to the Hasan-Boyce model for polymers, which has shown good agreement with other epoxy studies, to develop constitutive equations for these materials.

INTRODUCTION

Particulate composite materials composed of one or more varieties of particles in a polymer binder are widely used in military and civilian applications. They can be tailored for desired mechanical properties with appropriate choices of materials, particle sizes and loading densities. In this study, the effects of particle size and volume fraction on the mechanical properties of a model particulate composite, aluminum-filled epoxy are presented. Several studies on similar epoxy-based composites have been reported and have shown that particle size, shape [1], and concentration and properties of the constituents can affect the properties of particulate composites. In composites of Al_2O_3 particles in epoxy (Epon 828/Z), increasing the particle concentration and decreasing the particle size were found to increase the stress at 4% strain [2]. A study of aluminum filled epoxy (DGEBA/MTHPA) found adding a small amount of filler (~ 5 vol.%) increased the compressive yield stress, but additional amounts of filler decreased the compressive yield stress [3]. However, tests on epoxy (DOW DER 331/bisphenol-A) found that increasing the volume percent of glass bead filler increased the yield stress and fracture toughness of the material [4, 5].

EXPERIMENTAL PROCEDURE

Sample Characterization and Preparation

In this study, epoxy-based particulate composites, consisting of aluminum powder in an epoxy binder, were prepared, as detailed in Table 1. The epoxy binder is Shell Epon 826 with a DEA hardener. Characterization of the powders' particle size, surface area, and density was conducted. The particle size

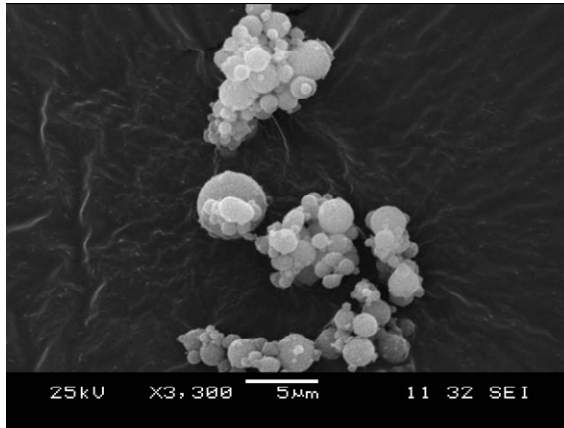
was determined using Mie light scattering with a Micromeritics Saturn Digisizer. The surface area was determined with a Micromeritics Gemini V using a static volumetric technique. A Quantachrome Ultrapycnometer 1000 was used to determine the density of the as-received powders. The results of the characterization are presented in Table 2. The as-received powders were examined with scanning electron microscopy (JEOL JSM 5900LV). Micrographs of the powders are presented in Figure 1 (a) and (b).

Table 1: Sample Description and Properties

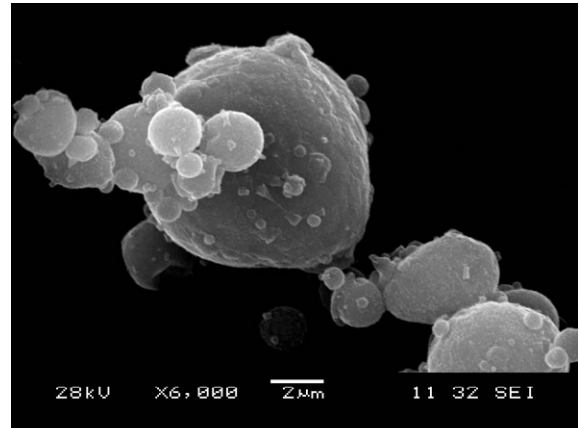
Sample	Description	Vol. % (Wt.%) Particles	Avg. Particle Size (μm)	Density [g/cm ³] (%TMD)
Epoxy-65H2	Shell Epon 826/DEA with Valimet H2 Al	46 (65)	3.5	1.862 (99)
Epoxy-65H5	Shell Epon 826/DEA with Valimet H5 Al	46 (65)	5.4	1.853 (99)

Table 2: Characterization of H2 and H5 aluminum powder

H2 Aluminum	H5 Aluminum
Surface Area (m ² /g)	
1.522 \pm 0.093	1.145 \pm 0.032
Particle Size (μm)	
3.479 \pm 0.042	5.425 \pm 0.076
Density (g/cm ³)	
2.720 \pm 0.012	2.688 \pm 0.009



(a)



(b)

Figure 1: SEM micrographs of (a) H2 Aluminum powder and (b) H5 Aluminum powder

Mechanical Properties Testing

All samples were tested in compression across a range of strain rates from 10^{-2} to 10^4 , at room temperature. An Instron model 1332 was used for quasi-static loading, in which the samples were nominally 8 mm diameter by 3.5 mm thick. It is generally accepted that quasi-static compression samples should have a length to diameter ratio of 2 : 1. However, in these experiments, samples with dimensions identical to those used for the split Hopkinson pressure bar were tested. The strain in the sample was determined from crosshead displacement, and the stress was determined from the load cell output. All data was acquired using Instron's Merlin software. Additionally, the particulate composite samples were tested in using a three point bending apparatus, according to ASTM Standard D790-03.

Compression experiments at intermediate strain rates ($10^3 - 10^4$) were conducted using two split Hopkinson pressure bars (SHPB) [6, 7]. The SHPB system is comprised of 1524 mm long, 19 mm diameter incident and transmitted bars of 440-HT stainless steel or 6061-T6 aluminum. The striker is 305 mm long and made of the same material as the other bars. The samples, which were nominally 8 mm diameter by 3.5 mm thick or 5 mm diameter by 2.5 mm thick, depending on strain rate, are positioned between the incident and transmitted bars. The bar faces were lightly lubricated with paraffin wax to reduce friction.

Experiments on epoxy samples at ultra-high strain rates (10^4 s^{-1}) were conducted using a miniaturized split Hopkinson pressure bar (MSHPB), which is, in principle, identical to the full sized SHPB. However, the bars are 300 mm long and 3 – 3.2 mm in diameter. Samples tested in this apparatus are nominally 1.5 mm diameter by 0.6 mm long. Miniaturized direct impact bar systems have been widely studied [8-10] and Jia and Ramesh [11] recently published a comprehensive analysis of a similar miniature bar system. A major advantage of the split bar system, over direct impact, is that mechanical equilibrium in the specimen may be conformed by comparing one- and two-wave analyses, as described by Gray [6]. The MSHPB provides the opportunity to test materials up to strain rates of 10^5 s^{-1} , with tungsten carbide (WC) and titanium alloy (Ti-6Al-4V) bar materials available.

For all bar systems, the properties of the sample are determined by measuring the incident, reflected, and transmitted strain signals, ε_i , ε_R , and ε_T respectively, using Kulite AFP-500-90 semiconductor strain gages. These gages are smaller (1 mm long) than traditional foil gages and have a much higher gage factor (140). The gages form part of a potential divider circuit with constant voltage excitation, which transforms the resistance change of the gages to a voltage change and compensates for temperature changes. The strain gages are dynamically calibrated in situ by performing a number of impacts with carefully measured striker bar velocities. From the measured impact velocity and mass of the striker, the force amplitude of the stress pulse introduced, F , can be determined and compared to the voltage output, V , from the strain gages to give a calibration in the form:

$$F = KV(1 + bV), \quad (1)$$

where K and b are calibration factors.

The full derivation of the data reduction used to calculate the strain rate and stress in the specimen, as functions of time, can be found in references [6, 7, 12]. In order to make representative measurements of material properties, it is necessary that the specimen achieves mechanical equilibrium during the experiment, and this is sometimes assumed as it makes the strain rate calculation more straightforward [6]. The software used in the experiments presented in this paper performs the one- and two- wave analyses automatically for every specimen, so stress state equilibrium can be verified in every experiment. However, the calculation of strain rate does not assume mechanical equilibrium, rather it uses all three of the incident, reflected and transmitted force pulses to calculate specimen strain rate through the following equation:

$$\dot{\varepsilon}(t) = \left[\frac{C_b}{l_s} \right] (\varepsilon_i(t) - \varepsilon_R(t) - \varepsilon_T(t)) \quad , \quad (2)$$

where ε_i , ε_R , and ε_T are the incident, reflected and transmitted strain pulses time shifted to the front and rear faces of the specimen, respectively, C_b is the sound speed in the bar material, and l_s is the length of the sample. This specimen strain rate is then integrated to give the strain,

$$\varepsilon(t) = \int_0^t \dot{\varepsilon}(t) dt \quad , \quad (3)$$

and the transmitted strain pulse is used to calculate the reported one-wave specimen stress,

$$\sigma(t) = \left[\frac{E_b A_b}{A_s} \right] \varepsilon_T(t), \quad (4)$$

where E_b , and A_b are the elastic modulus and cross-sectional area of the bar material, respectively, and A_s is the cross-sectional area of the sample. The two-wave specimen stress is calculated using Equation 4 with ε_T replaced by $\varepsilon_l + \varepsilon_R$. If true stress is required, A_s is typically updated using the strain calculation, assuming that volume is conserved during deformation.

Quantitative Microstructural Analysis

Previous work [13-18]. has shown that the spatial distribution of phases in particle-reinforced composite microstructures can have a significant effect on the mechanical properties of the material; including but not limited to strength [19, 20], ductility [21, 22], fatigue [23], damage evolution [24, 25], and fracture behavior [26, 27]. In order to provide quantifiable relationships between mechanical properties and microstructural attributes, detailed *quantitative* microstructural analysis must first be carried out. In this study, Scanning Electron Microscopy (SEM) was used to provide digital micrographs for this purpose. Secondary Electron Imaging (SEI) of metallographically-polished, carbon-coated specimens provided adequate contrast between the aluminum particles, the epoxy matrix and any porosity present after curing. The digital micrographs were obtained using a FEI Sirion microscope operating at 15kV, with 4Pi image acquisition system providing 1024×1024 pixel images at 16-bit depth.

Two different techniques for quantifying the composite microstructures were used in the present work; firstly, particle volume fractions and size distributions for the two materials (Epoxy-65H2 and Epoxy-65H5) were obtained using the commercially-available Clemex Vision® PE software; secondly, an in-house code (*MSAAF*: Multi-Scalar Analysis of Area Fractions) was employed in order to measure the level of microstructural homogeneity in each of the materials. Homogeneity was quantified using the negative slope of the *MSAAF* plot, according to the analysis of Spowart *et al* [20, 21, 28], as outlined below.

Multi-Scalar Analysis of Area Fractions (MSAAF)

This technique works by dividing up the microstructure into local grid squares and then measuring the coefficient of variation of local area fractions on that sectioning plane, $CV(A_i) = \sigma A_i / A_i$, where σA_i is the standard deviation of the individual local area fractions on the plane and A_i is their statistical mean. It has been previously shown that for a Poisson (random) distribution of mono-sized circular particles of diameter d_p , this statistical parameter should vary with grid size, Q , according to the following relationship, for $Q \gg d_p$,

$$CV(Q) = \left(\frac{\pi}{4A_f} \right)^{0.5} \left(\frac{Q}{d_p} \right)^{-1}. \quad (5)$$

When this relationship is plotted on a log-log scale (i.e. the *MSAAF* plot) the result is a straight line with a slope of -1 . In general, for any spatial distribution of mono-sized particles, the slope of the line is given by the parameter ξ , i.e.

$$\frac{d \log(CV)}{d \log(Q / d_p)} = -\xi. \quad (6)$$

The utility of this metric is that for microstructures that contain particles that are more clustered than the corresponding Poisson random case, $\xi > -1$; for microstructures that are more uniformly arranged, $\xi < -1$. Furthermore, the same overall relationship is also valid for moderately poly-dispersed particle distributions, as in the present case of the aluminum particles used to reinforce the epoxy matrix.

RESULTS AND DISCUSION

Epoxy Behavior and Comparison with Hasan-Boyce Model

Epoxy samples were tested at a range of strain rates from 1×10^{-2} to 38000 /s, as shown in Figure 2. It can be seen that the epoxy demonstrates a rise to a peak pressure, followed by strain softening, a region of nearly perfectly plastic flow, and strain hardening, which is comparable to behavior seen in similar epoxy materials [29]. The Hasan-Boyce model has been used for glassy polymers [29-31], and is described in detail in these references. Application of the Hasan-Boyce model depends on the appropriate choice of several constants, detailed in Table 3. As a first approximation, the constants derived by Lu, *et al* [29], for the same epoxy resin with a different curing agent, were used to compare to the experimental data in this study. It can be seen from Figure 2, that, although there is qualitative agreement, the model curves greatly over-predict the experimental behavior. This is hypothesized to be due to the difference in the epoxy strength using two different curing agents. Additional work is underway to optimize the Hasan-Boyce parameters for the particular epoxy used in this study.

Table 3: Constants used in Hasan-Boyce Model [29]

ω_0 (Hz)	$\dot{\gamma}_0$ (s ⁻¹)	ξ	λ (Å/m ³)	$\Delta v_{\tau 0}^*$ (Å ³)	α_0^{-1} (eV ⁻¹)
7.5×10^{11}	4.0×10^{10}	80	2	1090	1
α_{eq}^{-1} (eV ⁻¹)	a_0 (eV)	a_{eq} (eV)	β_1	β_2	β_3
1.67	0.877	0.800	9.0×10^{-3}	4.0×10^4	11.0×10^4

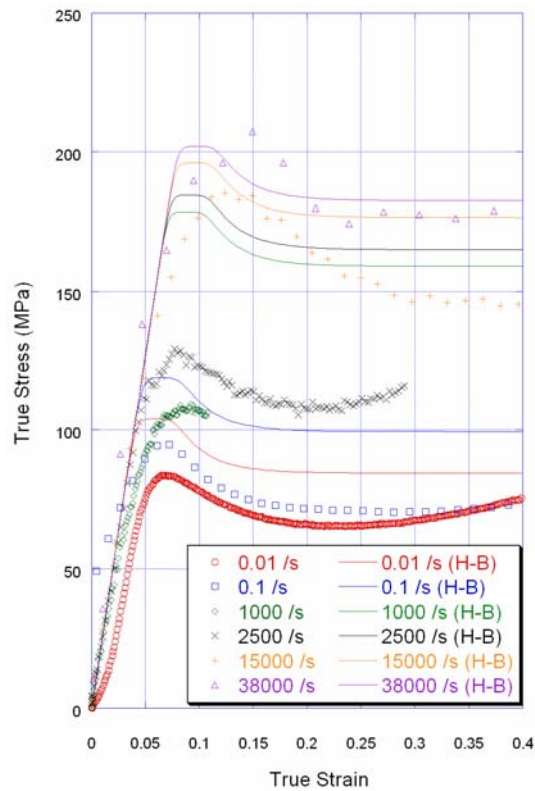


Figure 2: Compressive stress-strain behavior of Epon 826/DEA compared with Hasan-Boyce model using constants from Table 3

Epoxy – Aluminum Composites

The particulate composites, Epoxy-65H2 and Epoxy-65H5, have been formulated and testing is ongoing on these formulations. The materials have been tested in a static three point bend configuration as well as in compression, both statically and dynamically, with a summary of the results presented in Table 4. Flexural testing of these materials has revealed that both materials fail by particle pull out, i.e. the failure of the interface between the aluminum particles and the epoxy binder, as shown in Figure 3. Additionally, these materials fail in a brittle manner in tension, as evidenced by the lack of yield and flowing in the stress – strain curve. The lower flexural failure stress in the Epoxy-65H2 material, with a smaller aluminum particle size maybe due to a larger number of interfaces per unit volume. Alternatively, if one assumes a similar natural oxide layer thickness for both the H2 and H5 particles, the smaller (H2) aluminum particles will have a higher overall oxide-to-metal ratio than the larger (H5) particles, possibly lowering the overall composite strength. Although inconclusive on its own, the slightly higher density of the H2 powder (see Table 1) would also be consistent with this hypothesis.

The compressive stress-strain curves at three strain rates (0.001, 1.3, and 1150 /s) for both composites are presented in Figure 4 (a). Both materials show a rise to a “yield” stress followed by strain softening, a region of nearly perfectly plastic flow, and then a region of strain hardening. This is similar to the behavior of the epoxy binder material, indicating that the properties of the binder are dominating in compression. At all three strain rates, the smaller particle size material (Epoxy-65H2) has consistently higher strength. A plot of the “yield” or peak stress for both materials versus log strain rate, Figure 4 (b), reveals a nearly straight line, which indicates that the epoxy binder is not undergoing any phase transitions in this strain rate regime.

Table 4: Summary of mechanical testing data on Epoxy-65H2 and Epoxy-65H5

Material	$\langle d_p \rangle$ (μm)	E (GPa)	σ_{fail} (MPa)	$\sigma_{\text{peak}} (\dot{\epsilon} = 10^{-3})$ (MPa)	$\sigma_{\text{peak}} (\dot{\epsilon} = 10^0)$ (MPa)	$\sigma_{\text{peak}} (\dot{\epsilon} = 10^3)$ (MPa)
Epoxy-65H2	3.5	0.92 ± 0.05	8.0 ± 0.8	101 ± 0.7	127 ± 0.4	170 ± 4
Epoxy-65H5	5.4	0.83 ± 0.03	9.6 ± 0.5	95 ± 0.1	117 ± 0.2	150 ± 2

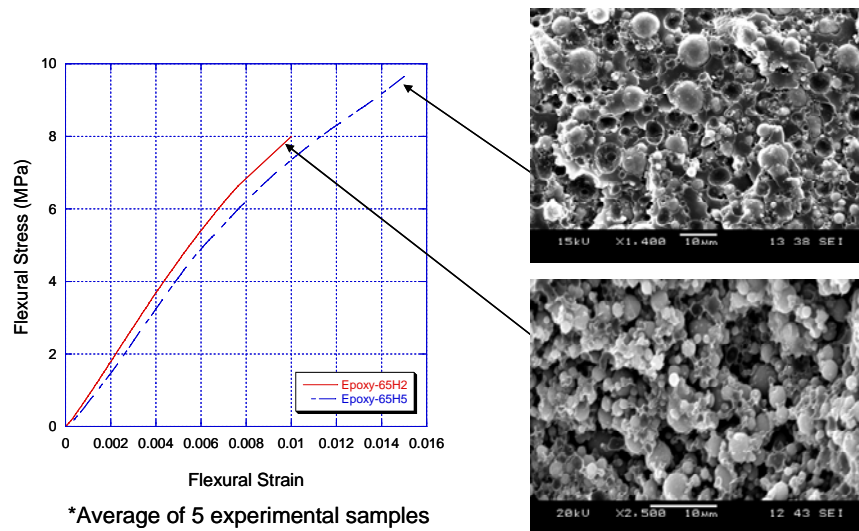


Figure 3: Flexural testing results and associated fracture surface micrographs of Epoxy-65H2 and Epoxy-65H5.

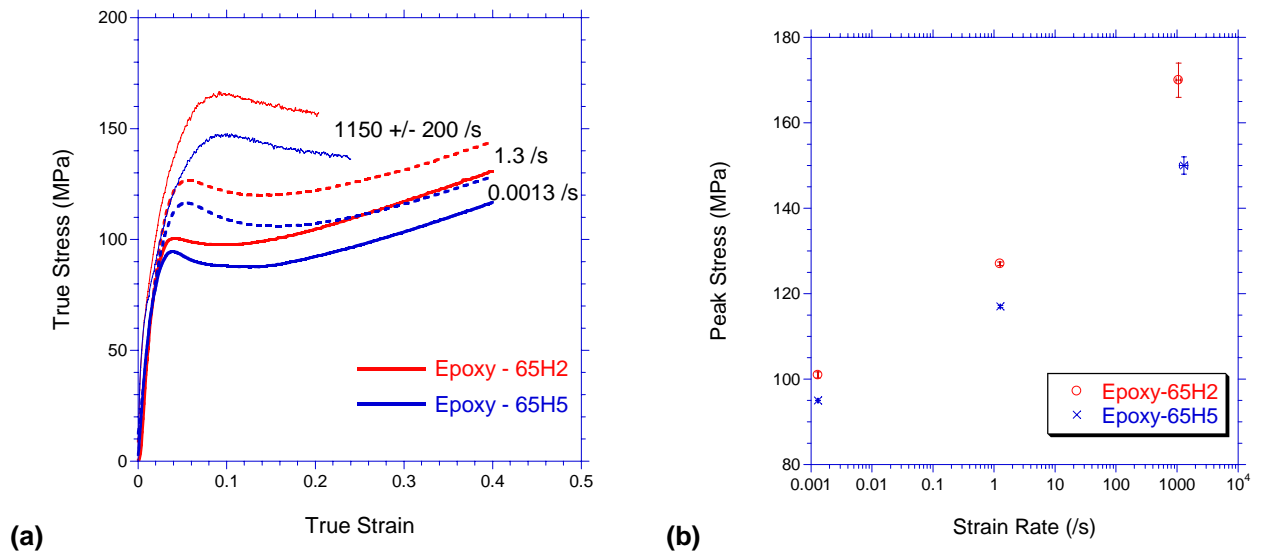


Figure 4: (a) Compressive stress-strain curves for Epoxy-65H2 and Epoxy-65H5 at quasi-static and dynamic strain rates and (b) peak stress versus log strain rate for both composites.

Quantitative Microstructural Analysis

Figures 5(a) and 5(b) show typical SEM micrographs of the as-polished Epoxy-65H2 and Epoxy-65H5 composite specimens. These images were obtained using SEI contrast, and clearly show the 3 major constituents of the microstructure; epoxy matrix (dark gray), aluminum particles (light gray) and pores (black). In addition to these, there is evidence of particle pull-out during polishing, as characterized by the dark gray features with bright halation due to charging under the electron beam. However, due to uncertainty in their exact origin, these features were ignored in the statistical particle-counting process, which may lead to an under-representation of the true particle volume fraction, to be discussed later.

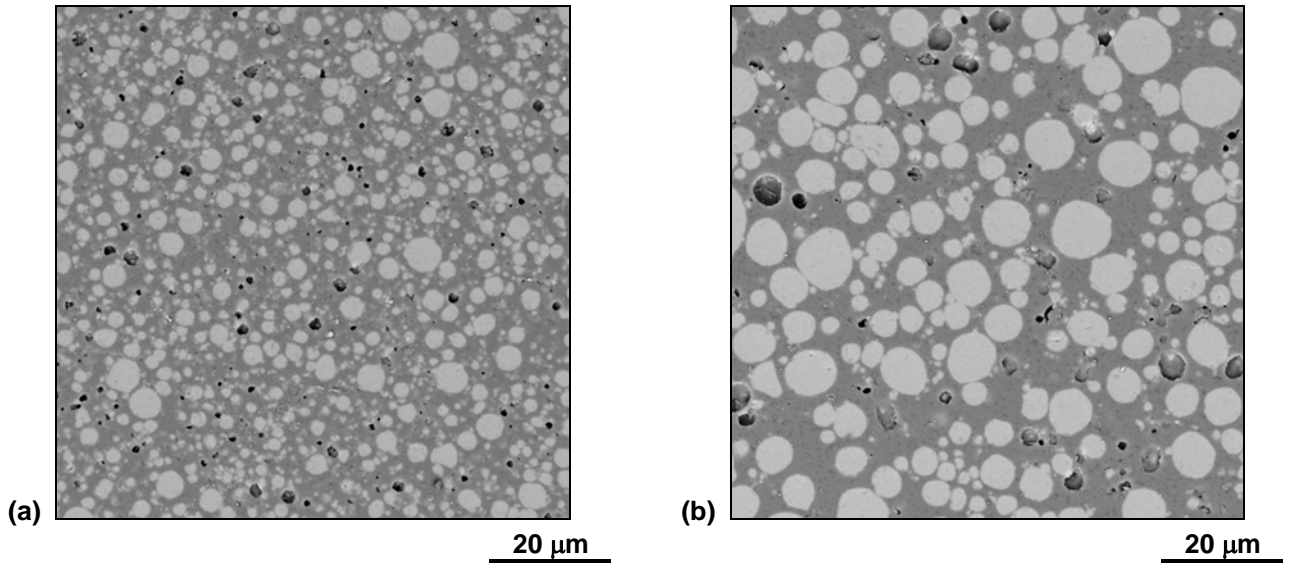


Figure 5: Typical SEM micrographs of as-polished epoxy-aluminum composite specimens; (a) Epoxy-65H2; (b) Epoxy-65H5. Images obtained with SEI contrast clearly show epoxy matrix (dark gray), aluminum particles (light gray) and small pores (black). Dark gray features with bright halation are evidence of particle pull-out during polishing.

The microstructures in Fig. 5 were gray-level thresholded using the Clemex Software, to obtain the following binary images where the black features are the aluminum particles and the white background is the epoxy matrix, Fig. 6. Binarization of the images allows the particle size statistics and area (volume) fraction measurements to be made automatically, using the same software. In addition, the binary images were used as input into the MSAAF code in order to measure the levels of microstructural homogeneity in each specimen.

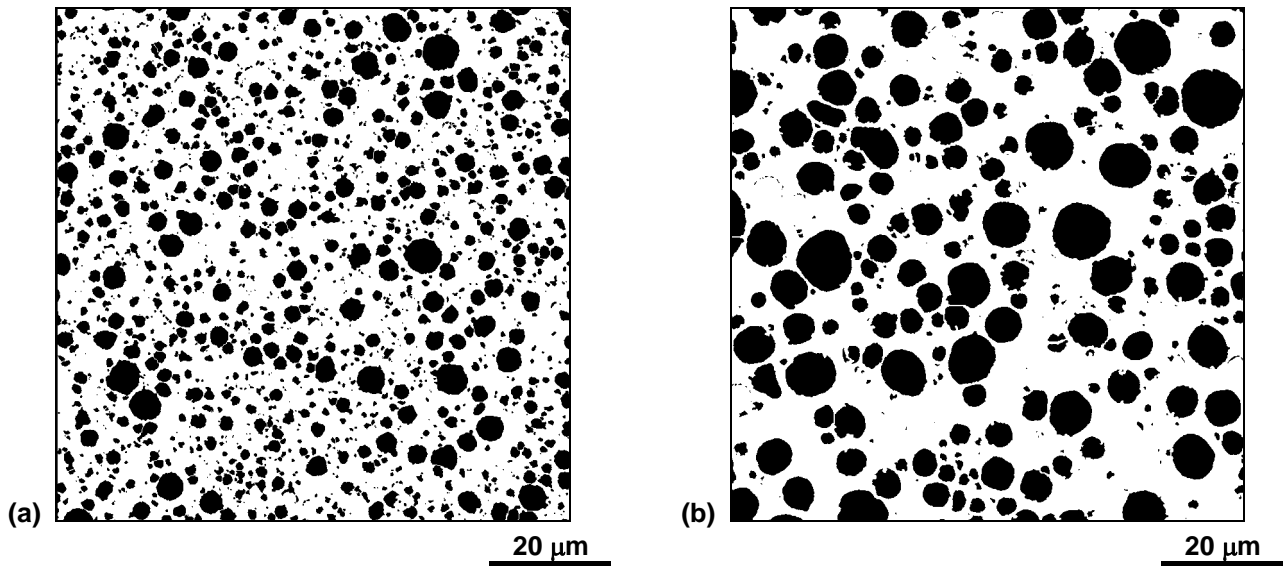


Figure 6: Binarized (thresholded) images of the aluminum-epoxy composite specimens; (a) Epoxy-65H2; (b) Epoxy-65H5. These images were used to obtain particle size statistics, overall area (volume) fractions of particles using the Clemex software and formed the basis of the MSAAF analysis for microstructural homogeneity. Black features are aluminum particles and white background is the epoxy matrix.

The overall area (volume) fractions of the aluminum reinforcement were measured from these binarized images. For the Epoxy-65H2 and Epoxy-65H5 composites, $A_f (=V_f) = 0.32$ and 0.38 , respectively. These volume fractions differ significantly from the expected values of 0.45 , based on the information in Table 1. It is postulated that this discrepancy is primarily due to those particles which are pulled-out during metallographic preparation not being counted in the statistical analysis. In addition, statistical particle size analysis using the same thresholded images gave mean equivalent spherical particle sizes for the Epoxy-65H2 and Epoxy-65H5 composites of $2.4 \pm 0.5 \mu\text{m}$ and $5.5 \pm 0.6 \mu\text{m}$, respectively, as shown in Figures 7(a) and 7(b). Although the mean equivalent spherical particle size for the Epoxy-65H5 specimen is in good agreement with the value of $\langle d_p \rangle$ measured directly from Mie light scattering, this is not the case for the Epoxy-65H2 specimen. In addition, there is significantly more experimental error in the measurement made on the images, than that from light scattering, possibly due to fewer particles being sampled. The difference between the two measures of particle size can be explained by the higher levels of porosity observed in the Epoxy-65H2 specimen, which, due to thresholding can be erroneously included as a population of smaller particles, thereby dragging down the mean. Fig. 8 shows the typical, small-scale porosity that was observed in each material. For the Epoxy-65H2 specimen, the pore fraction was measured at 0.007 , almost twice that of the Epoxy-65H5 specimen, at 0.003 . Moreover, the increased levels of porosity in the Epoxy-65H2 specimen may have contributed to a small extent to the larger under-prediction of the overall area (volume) fraction in this material than in the Epoxy-65H5 material.

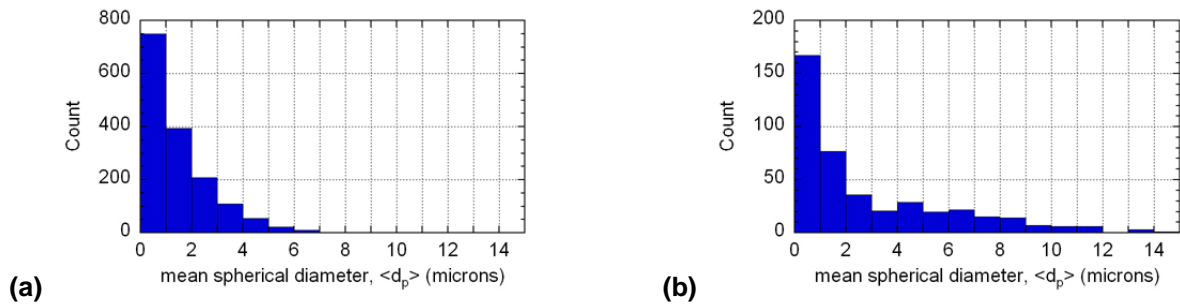


Figure 7: Particle size analysis from binarized images; (a) Epoxy-65H2; (b) Epoxy-65H5.

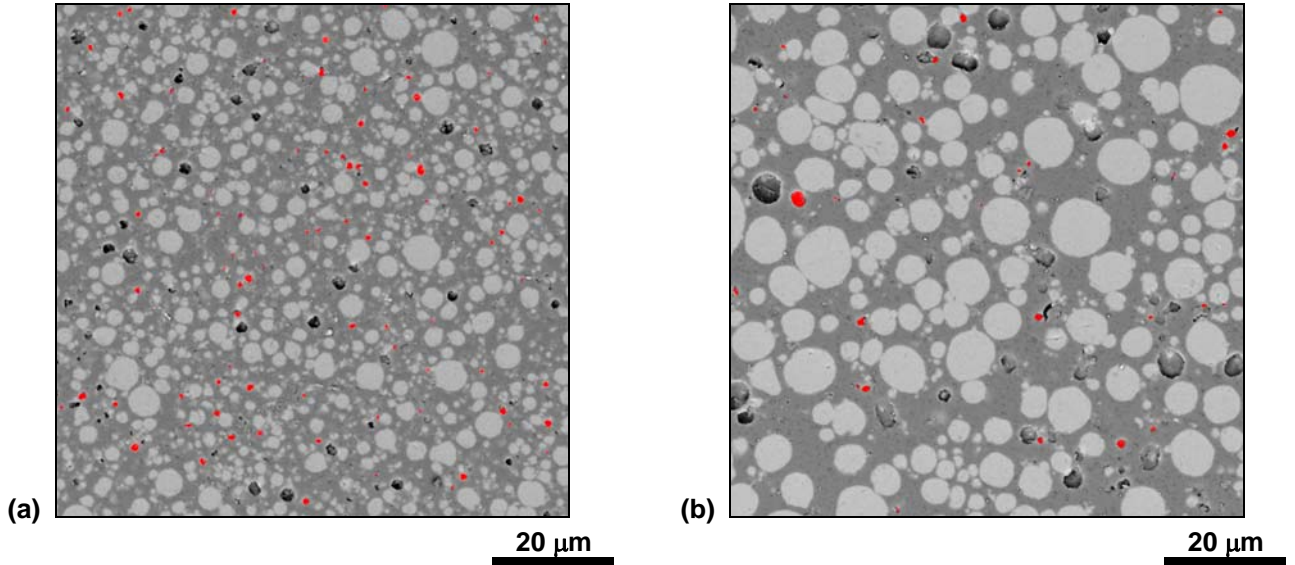


Figure 8: Images showing the porosity present in the aluminum-epoxy composite specimens; (a) Epoxy-65H2; (b) Epoxy-65H5. The red features are pores superposed on the epoxy matrix with aluminum particles. Overall pore fractions were measured to be $P_f = 0.007$ (Epoxy-65H2) and $P_f = 0.003$ (Epoxy-65H5).

The level of microstructural homogeneity present in each microstructure is very similar. The slopes of the MSAAF plots generated from the Epoxy-65H2 and Epoxy-65H5 materials were calculated to be -0.96 ± 0.01 and -0.97 ± 0.01 , respectively. Effectively, the slope of the MSAAF plot is a quantitative indicator of how randomly the particles are arranged in space. A slope of -1.00 indicates perfectly random, non-overlapping placement of particles; slopes that are more positive indicate increasing degrees of particle clustering; and slopes that are more negative indicate a predisposition for the particles to be well-separated, as if by repulsive forces. Hence, in these aluminum-epoxy composite materials, the particles are only very slightly clustered, possibly due to attractive forces operating during the cast-cure processing or due to the presence of the small satellite particles, as previously indicated in Figs 1(a) and (b). In all other respects, the particles have been well-dispersed throughout the matrix by the mixing process.

SUMMARY

Two particulate composites, Epoxy-65H2 and Epoxy-65H5, have been prepared and mechanically characterized using static flexural testing and static and dynamic compression testing. In tension, as loaded in the flexural test, both materials failed at the interface between the aluminum particles and the epoxy binder. The smaller particle size sample (Epoxy-65H2) showed a lower flexural failure stress perhaps due to; (i) the increase in number of interfaces per unit volume; or (ii) the greater oxide component in the smaller aluminum particles. In compression, the smaller particle size sample was consistently

stronger than the larger particle size sample due to the larger number of particles per unit volume, which constrain the epoxy flow behavior. The difference in the compression and tension behavior of these materials reveals that the interface is weak compared to the strength of the matrix. Microstructurally, both composites were similar in terms of their microstructural homogeneity, which was consistently high. However, the Epoxy-65H2 material revealed higher porosity levels than the Epoxy-65H5 material. Careful thresholding and binarization is needed in order to provide volume fraction and particle size measurements that are consistent with those from the other techniques. Specifically, particle pull-out during metallographic polishing should be minimized in order to suppress image artifacts that can arise due to thresholding.

ACKNOWLEDGEMENTS

This research was sponsored by the Air Force Office of Scientific Research (Brett Conner, Program Manager) and the Air Force Research Laboratory, Munitions Directorate.

Opinions, interpretations, conclusions and recommendations are those of the authors and are not necessarily endorsed by the United States Air Force.

REFERENCES

1. Ramsteiner, F. and Theysohn, R. (1984): "On the tensile behavior of filled composites," *Composites*, Vol. 15, pp. 121-128.
2. Oline, L.W. and Johnson, R. (1971): "Strain Rate Effects in Particulate-Filled Epoxy," *Proceedings of ASCE: Journal of the Engineering Mechanics Division*, Vol. 97 [EM 4], pp. 1159-1172.
3. Goyanes, S., Rubiolo, G., Marzocca, A., Salgueiro, W., Somoza, A., Consolati, G., and Mondragon, I. (2003): "Yield and internal stresses in aluminum filled epoxy resin. A compression test and positron annihilation analysis," *Polymer*, Vol. 44, pp. 3193-3199.
4. Kawaguchi, T. and Pearson, R.A. (2003): "The effect of particle-matrix adhesion on the mechanical behavior of glass filled epoxies: Part 1. A study on yield behavior and cohesive strength," *Polymer*, Vol. 44, pp. 4229-4238.
5. Kawaguchi, T. and Pearson, R.A. (2003): "The effect of particle-matrix adhesion on the mechanical behavior of glass filled epoxies: Part 2. A study on fracture toughness," *Polymer*, Vol. 44, pp. 4239-4247.
6. Gray III, G.T., *Classic split-Hopkinson pressure bar testing*, in *ASM Handbook. Vol 8: Mechanical Testing and Evaluation*, H. Kuhn and D. Medlin, Editors. 2002, ASM International: Materials Park. p. 462-476.
7. Tasker, D.G., R.D. Dick, and W.H. Wilson. *Mechanical Properties of Explosives Under High Deformation Loading Conditions*. in *Shock Compression of Condensed Matter - 1997*. 1998: American Institute of Physics.
8. Gorham, D.A., *Measurement of stress-strain properties of strong metals at very high rates of strain*. Institute of Physics Conference Series, 1979. **47**: p. 16-24.
9. Gorham, D.A., P.H. Pope, and J.E. Field, *An improved method for compressive stress strain measurement at very high strain rates*. Proceedings of the Royal Society of London, 1992. **438**: p. 153-170.
10. Mentha, S.N., P.H. Pope, and J.E. Field, *Progress in metal testing with a 3 mm pressure bar*. Institute of Physics Conference Series, 1984. **70**: p. 175-176.
11. Jia, D. and K.T. Ramesh, *A Rigorous Assessment of the Benefits of Miniaturization in the Kolsky Bar System*. Experimental Mechanics, 2004. **44**: p. 445-454.
12. Tasker, D.G., R.D. Dick, and W.H. Wilson. *Mechanical Properties of Explosives Under High Deformation Loading Conditions*. in *Shock Compression of Condensed Matter - 1997*. 1997: American Institute of Physics.

13. J. E. Spowart, Z.-Y. Ma, R. S. Mishra, The Effect of Friction Stir Processing (FSP) on the Spatial Heterogeneity of Discontinuously-Reinforced Aluminum (DRA) Microstructures, in: K. V. Jata, M. Mahoney, R. S. Mishra (Eds.), *Friction Stir Welding and Processing II*, TMS, Warrendale, PA, 2003, pp. 243-252.
14. S. F. Corbin, D. S. Wilkinson, *Acta. Metall. Mater.* 42 (1994) 1311-1318.
15. A. M. Murphy, S. J. Howard, T. W. Clyne, *Mat. Sci. Tech.* 14 (1998) 959-968.
16. A. R. Vaida, J. J. Lewandowski, *Mat. Sci. Eng. A220* (1996) 85-92.
17. S. Tao, J. D. Boyd, Mechanisms of Damage Accumulation and Fracture in Particulate Reinforced Metal-Matrix Composites, in: *Proceedings of the ASM 1993 Materials Congress*, ASM International, Materials Park, OH, Pittsburgh, PA, 1993, pp. 29-40.
18. J. J. Lewandowski, C. Liu, *Mat. Sci. Eng. A107* (1989) 241-255.
19. Bhanu Prasad, V.V., et al., *Structure-Property Correlation in Discontinuously-Reinforced Aluminium Matrix Composites as a Function of Relative Particle Size Ratio*. *Mat. Sci. Eng.*, 2002. **A337**: p. 179-186.
20. Spowart, J.E., B. Maruyama, and D.B. Miracle, *Multi-Scale Characterization of Spatially Heterogeneous Systems: Implications for Discontinuously-Reinforced Metal-Matrix Composite Microstructures*. *Mat. Sci. Eng. (A)*, 2001. **A307**: p. 51-66.
21. Spowart, J.E., Z.-Y. Ma, and R.S. Mishra, *The Effect of Friction Stir Processing (FSP) on the Spatial Heterogeneity of Discontinuously-Reinforced Aluminum (DRA) Microstructures*, in *Friction Stir Welding and Processing II*, K.V. Jata, M. Mahoney, and R.S. Mishra, Editors. 2003, TMS: Warrendale, PA. p. 243-252.
22. Murphy, A.M., S.J. Howard, and T.W. Clyne, *Characterisation of Severity of Particle Clustering and its Effect on Fracture of Particulate MMCs*. *Mat. Sci. Tech.*, 1998. **14**(Sept-Oct): p. 959-968.
23. Vaida, A.R. and J.J. Lewandowski, *Effects of SiCp Size and Volume Fraction on the High-Cycle Fatigue Behavior of AZ91D Magnesium Alloy Composites*. *Mat. Sci. Eng.*, 1996. **A220**: p. 85-92.
24. Jeni, M. and M. Kukuchi, *Damage Analysis of Al-Matrix Composite Considering Non-Uniform Distribution of SiC Particles*. *Acta mater.*, 1998. **46**: p. 3125-3133.
25. Lepinoux, J.L. and Y. Estrin, *Mechanical Behavior of Alloys Containing Heterogeneously-Distributed Particles*. *Acta mater.*, 2000. **48**: p. 4337-4347.
26. Lewandowski, J.J. and C. Liu, *Effects of Matrix Microstructure and Particle Distribution on Fracture of an Aluminum Metal Matrix Composite*. *Mat. Sci. Eng.*, 1989. **A107**: p. 241-255.
27. Tao, S. and J.D. Boyd. *Mechanisms of Damage Accumulation and Fracture in Particulate Reinforced Metal-Matrix Composites*. in *Proceedings of the ASM 1993 Materials Congress*. 1993. Pittsburgh, PA: ASM International, Materials Park, OH.
28. Spowart, J.E., *Microstructural Characterization and Modeling of Discontinuously-Reinforced Aluminum Composites*. *Mat. Sci. Eng.*, 2006, **A425**: p. 225-237.
29. Lu, H., G. Tan, and W. Chen. *Modeling of constitutive behavior for Epon828/T-403 at high strain rates*. *Mech. Time-Dependant Matl.* 2001. **5** (2): p. 119-130.
30. Hasan, O.A. and M. C. Boyce. *A constitutive model for the nonlinear viscoelastic viscoplastic behavior of glassy polymers*. *Polymer Eng. & Sci.* 1995. **35** (4): p. 331-344.
31. Austin, R., *Numerical Simulation of the Shock Compression of Microscale Reactive Particle Systems*. Master's Thesis. Georgia Institute of Technology. 2005.

HIGH STRAIN RATE MECHANICAL PROPERTIES OF EPOXY AND EPOXY-BASED PARTICULATE COMPOSITES

Jennifer L. Jordan¹, Jonathan E. Spowart², D. Wayne Richards¹, Bradley White³, and Naresh N. Thadhani³

¹AFRL/MNME, Air Force Research Laboratory, Eglin AFB, FL 32542

²AFRL/MLLMD, Air Force Research Laboratory, Wright-Patterson AFB, OH 45433

³School of Materials Science and Engineering, Georgia Institute of Technology, Atlanta, GA 30332



2007 Annual Conference and Exposition

June 3 – 6, 2007

DISTRIBUTION A; Approved for public release; Distribution Unlimited.



Outline



- **Background**
- **Objective and Approach**
- **Experimental Procedure**
- **Results and Discussion**
 - **Powder Characterization**
 - **Microstructural Characterization**
 - **Mechanical Characterization**
- **Summary**



Particulate Composites



- **Particulate composites consist of individual particles of one material dispersed throughout and held together by the other. Mechanical and physical properties of the composite depend on:**
 - **Mechanical and physical properties of individual components**
 - **Loading density (volume or mass fraction)**
 - **Particle size**
 - **Particle shape**
 - **Interfacial adhesion, *interphase* properties**
 - **Residual stresses from processing**
 - **Porosity**

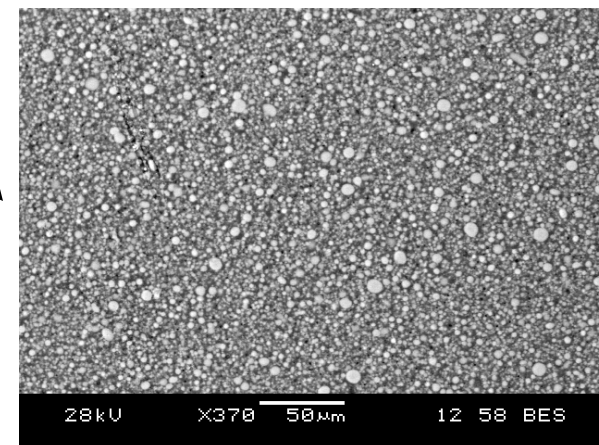
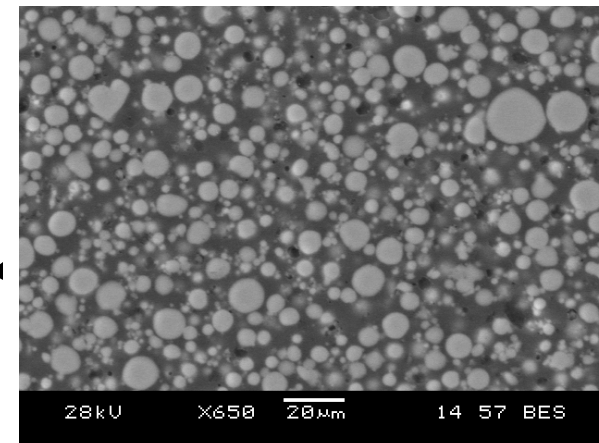


Objective and Approach



Objective: (1) To quantify the compressive mechanical properties in epoxy and compare with Mulliken – Boyce constitutive model and (2) to investigate microstructure-properties relationships in two cast-cure aluminum-epoxy composites made with two different grades of Al powder.

Sample	Description	Vol. % (Wt.%) Particles	Avg. Particle Size (μm)	Density [g/cm ³] (%TMD)
Epoxy-65H2	Shell Epon 826/DEA with Valimet H2 Al	46 (65)	3.5	1.862 (99)
Epoxy-65H5	Shell Epon 826/DEA with Valimet H5 Al	46 (65)	5.4	1.853 (99)





Experimental Procedure



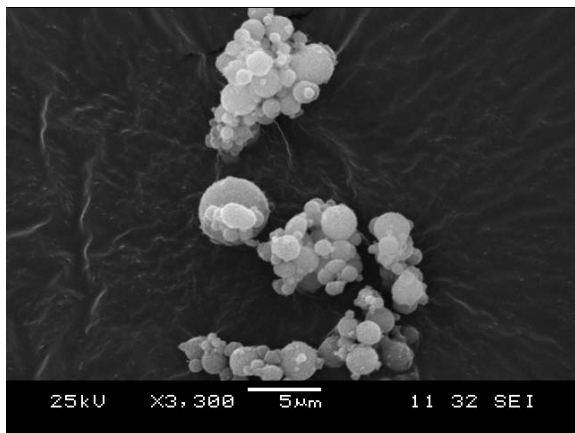
- **Particle Characterization**
- **Mechanical Characterization of Epoxy Binder and Comparison with Constitutive Model**
- **Microstructural Characterization of Composites**
- **Mechanical Characterization of Composites**
 - **Quasi-static flexural testing (Three point bend configuration)**
 - **Quasi-static compression testing**
 - **Dynamic compression testing (Split Hopkinson Pressure Bar)**



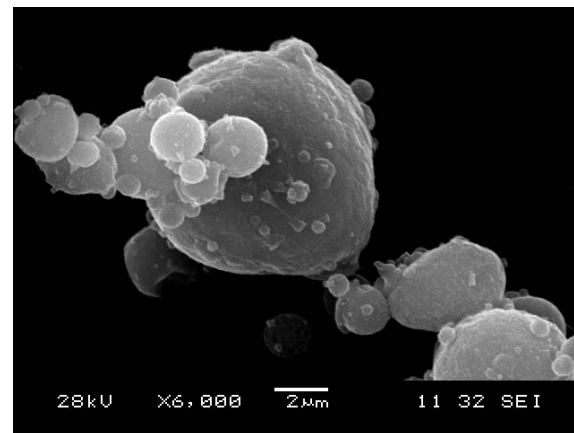
Powder Characterization



H2 Aluminum



H5 Aluminum



H2 Aluminum

H5 Aluminum

Surface Area (m ² /g)	
1.522 ± 0.093	1.145 ± 0.032
Particle Size (µm)	
3.479 ± 0.042	5.425 ± 0.076
Density (g/cm ³)	
2.720 ± 0.012	2.688 ± 0.009



Mulliken – Boyce Constitutive Model¹ (1-D)

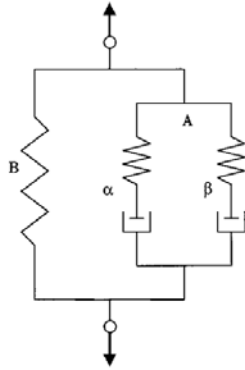


Fig. 14. A one-dimensional rheological interpretation of the proposed constitutive model for rate-dependent thermoplastic behavior.

$$\sigma = \sigma_{A\alpha} + \sigma_{A\beta} + \sigma_B$$

- **Langevin Spring – entropic resistance to chain alignment**
- **Viscoelastic Spring and Dashpot – intermolecular resistance to chain segment rotation**
 - **Alpha process: main-chain polymer segments**
 - **Beta process (epoxy): relaxations of glyceryl or diphenylpropane groups^{2,3}**

• Langevin Spring (B)

$$\sigma_B = \frac{C_R}{3} \frac{\sqrt{N}}{\lambda_p^{chain}} L^{-1} \left(\frac{\lambda_{chain}^p}{\sqrt{N}} \right) \left(e^\varepsilon - \frac{e^{2\varepsilon} + 2e^{-2\varepsilon}}{3} \right)$$

• Viscoelastic Spring and Dashpot (A)

$$\dot{\gamma}_\alpha^p = \dot{\gamma}_{0,\alpha}^p \exp \left[-\frac{\Delta G_\alpha}{k\theta} \left(1 - \frac{\tau_\alpha}{s_\alpha + \alpha_{p,\alpha} p} \right) \right]$$

$$\dot{\gamma}_\beta^p = \dot{\gamma}_{0,\beta}^p \exp \left[-\frac{\Delta G_\beta}{k\theta} \left(1 - \frac{\tau_\beta}{s_\beta + \alpha_{p,\beta} p} \right) \right]$$

$$\dot{s}_\alpha = h_\alpha \left(1 - \frac{s_\alpha}{s_{ss,\alpha}} \right) \dot{\gamma}_\alpha^p \quad \dot{s}_\beta = h_\beta \left(1 - \frac{s_\beta}{s_{ss,\beta}} \right) \dot{\gamma}_\beta^p$$

$$s_{0,\beta} \equiv \frac{0.077\mu_\beta}{1 - \nu_\beta}$$

$$s_{0,\alpha} \equiv \frac{0.077\mu_\alpha}{1 - \nu_\alpha}$$

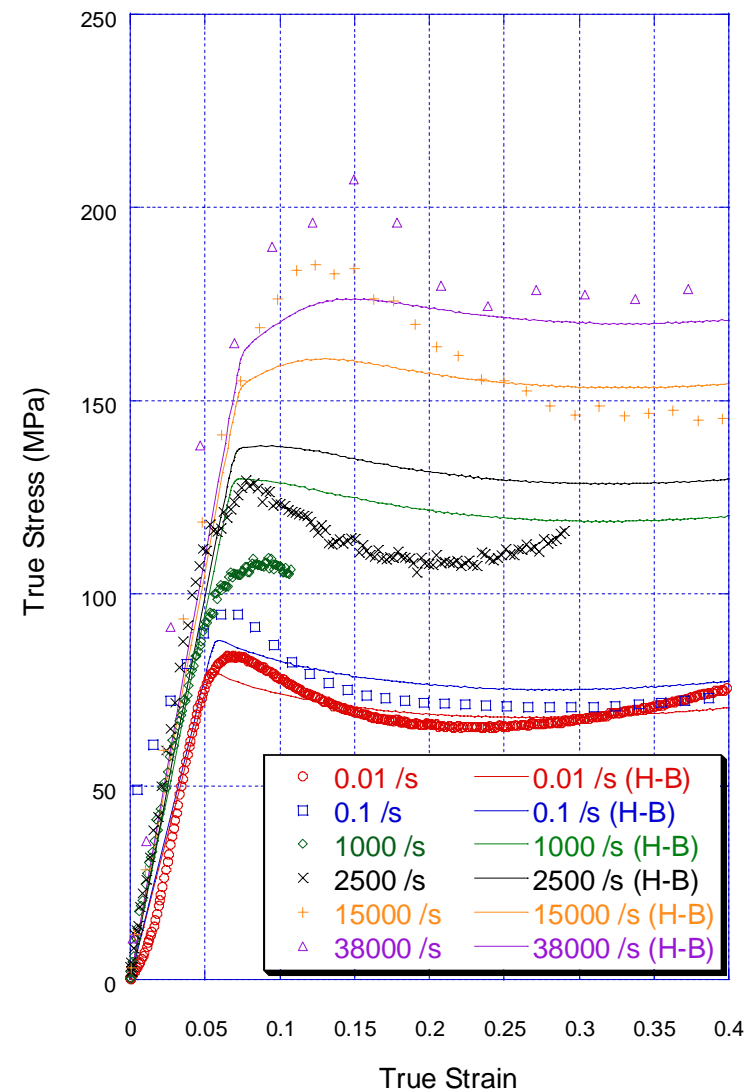
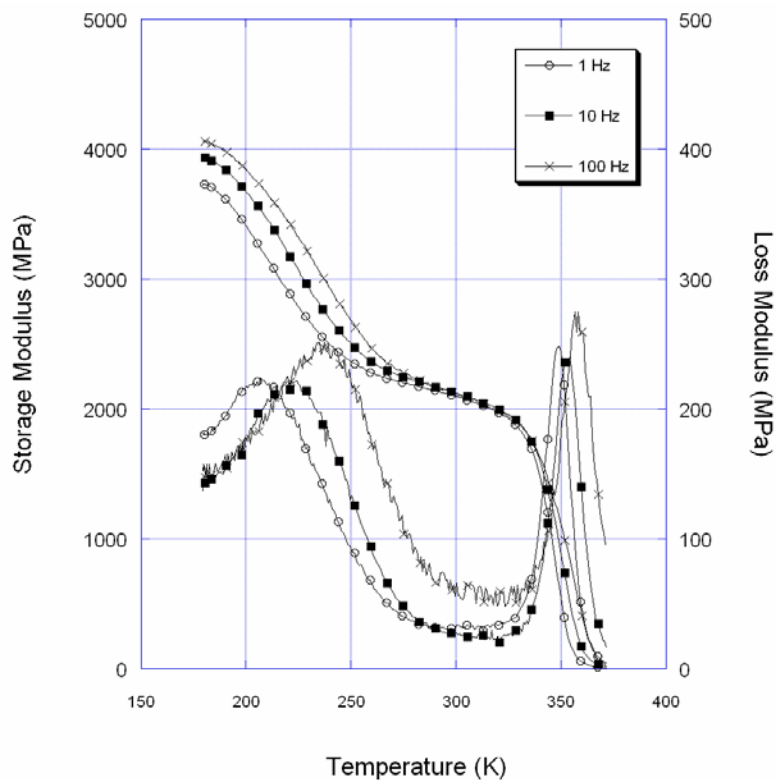
$$\dot{\sigma}_\alpha = E_\alpha \left(\dot{\varepsilon} - \dot{\varepsilon}_\alpha^p \right) \quad \dot{\sigma}_\beta = E_\beta \left(\dot{\varepsilon} - \dot{\varepsilon}_\beta^p \right)$$

References:

1. Mulliken, A.D. and M.C. Boyce, *Mechanics of the rate-dependent elastic-plastic deformation of glassy polymers from low to high strain rates*. International Journal of Solids and Structures, 2006. **43**(5): p. 1331-1356.
2. Foreman, J.P., et al., *Thermodynamic and mechanical properties of amine-cured epoxy resins using group interaction modeling*. Journal of Materials Science, 2006. **40**: p. 6631-6638.
3. Williams, J.G., *The Beta Relaxation in Epoxy Resin-Based Networks*. Journal of Applied Polymer Science, 1979. **23**: p. 3433-3444.



Mechanical Characterization of Epoxy and Comparison with Mulliken-Boyce Model



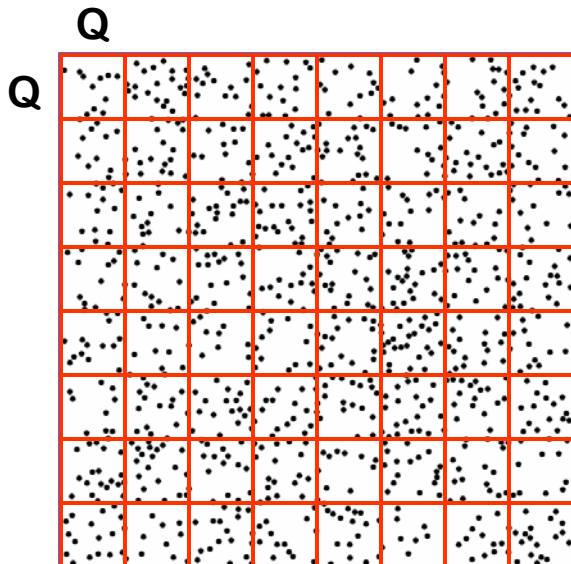


Multi-Scalar Analysis of Area Fractions (MSAAF)



For a “Poisson” random particle distribution:

- low area fraction, A_f
- small particle diameter, d_p
- mean number of particles in quilt area ($Q \times Q$) = n
- standard deviation of number of particles in quilt area ($Q \times Q$) = $n^{0.5}$



mono-sized disks, $A_f = 10\%$
random, non-overlapping
placement

$$n(Q) = \frac{A_f Q^2}{\pi d_p^2/4}$$

$$CV(Q) = n^{-0.5} = \left(\frac{\pi}{4A_f} \right)^{0.5} \left(\frac{Q}{d_p} \right)^{-1}$$

slope: $\frac{d \log(CV)}{d \log(Q/d_p)} = -1$

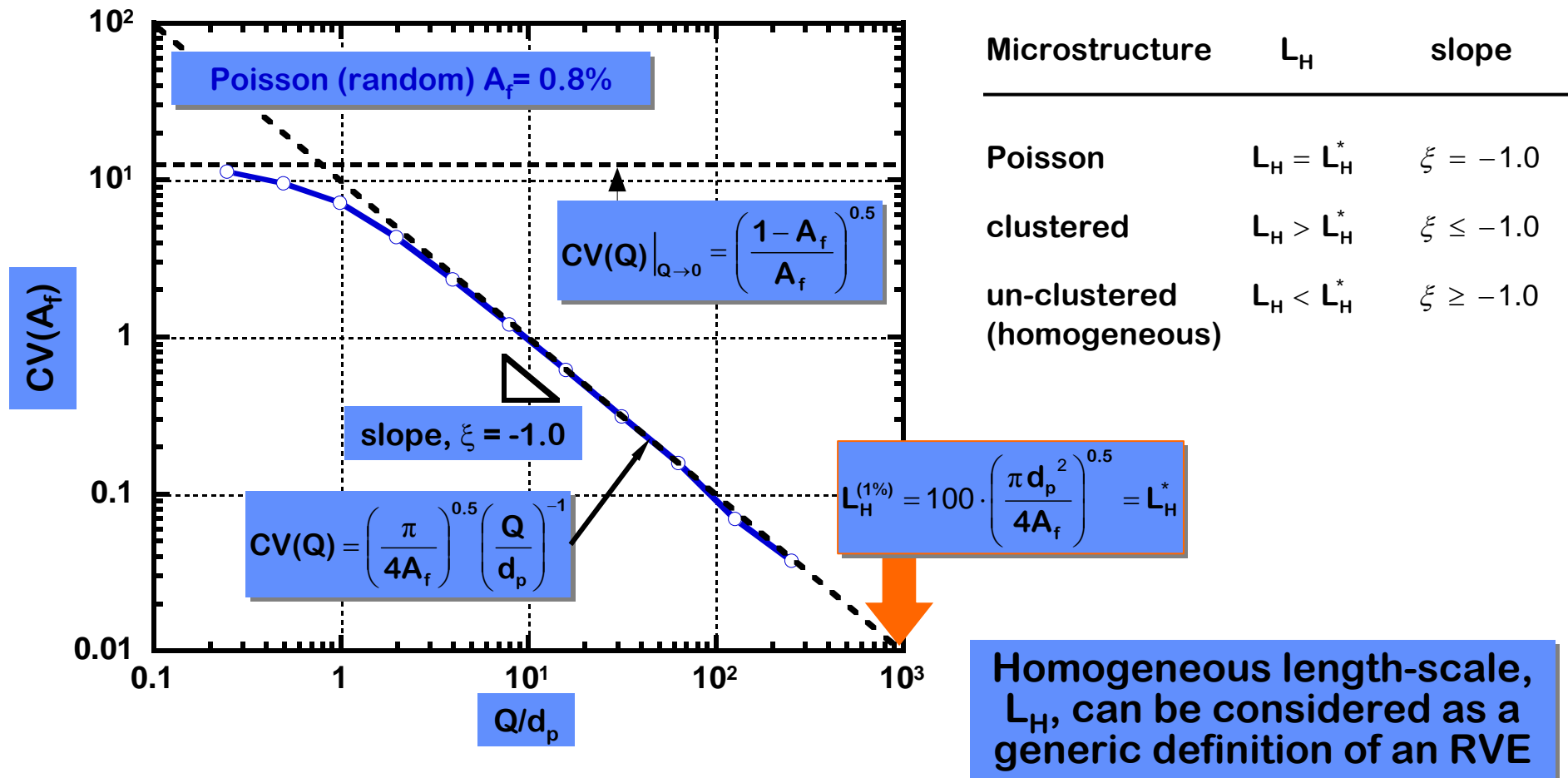
asymptote: $CV(Q)|_{Q \rightarrow 0} = \left(\frac{1 - A_f}{A_f} \right)^{0.5}$



Quantifying Spatial Heterogeneity



MSAAF plots for Poisson random microstructures¹



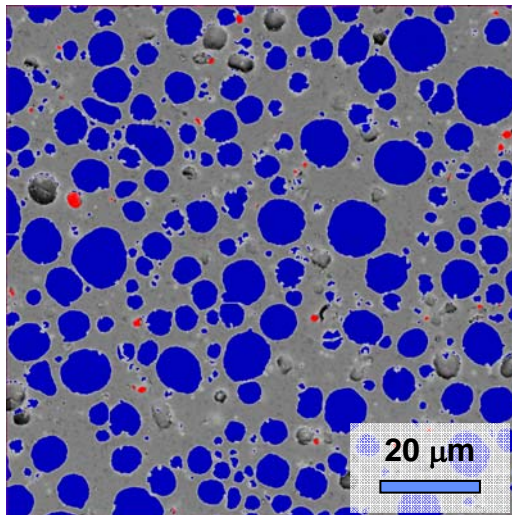
¹ J.E. Spowart, B. Maruyama and D.B. Miracle, Mat. Sci. Eng. (A), A307, pp. 51-66 (2001)



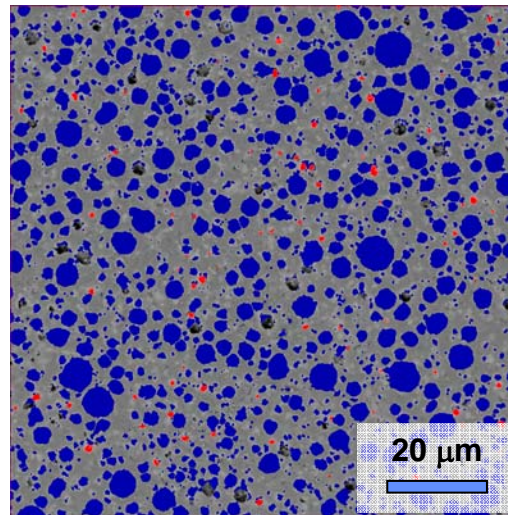
Microstructural Analysis



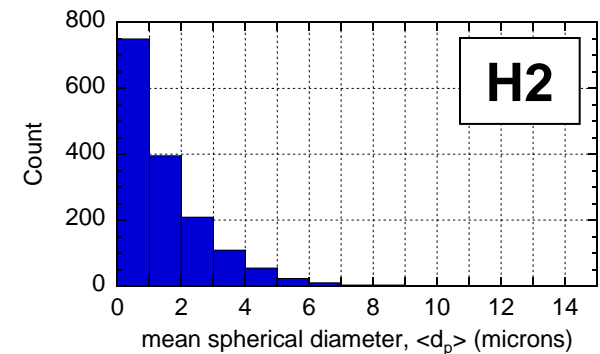
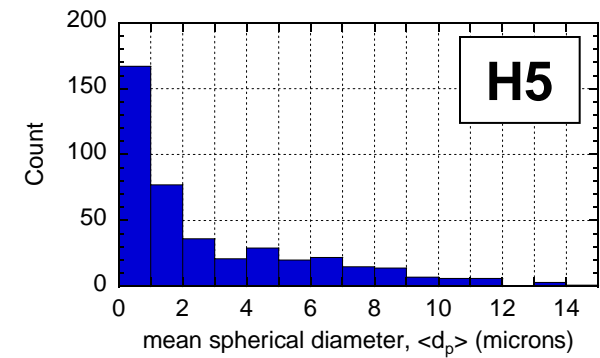
Cast-cure aluminum-epoxy composites made with two different grades of Al powder



Epoxy-65H5
 $\langle d_p \rangle = 5.5 \mu\text{m}$
 $V_f = 0.38$
 $P_f = 0.005$



Epoxy-65H2
 $\langle d_p \rangle = 2.4 \mu\text{m}$
 $V_f = 0.32$
 $P_f = 0.007$



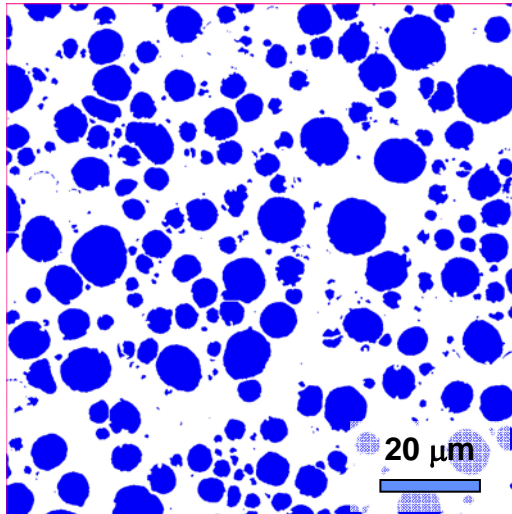
Robust quantification relies on artifact-free image analysis



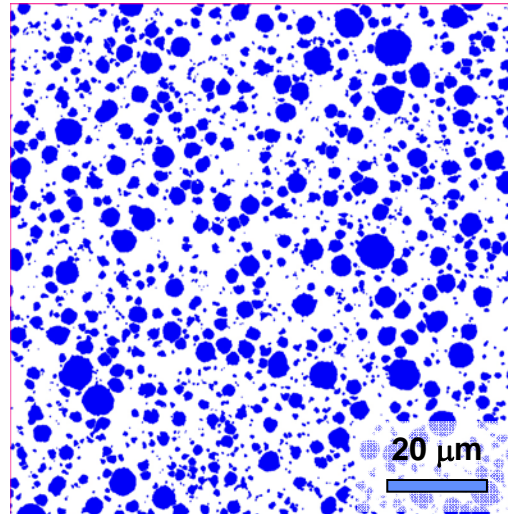
MSAAF Analysis



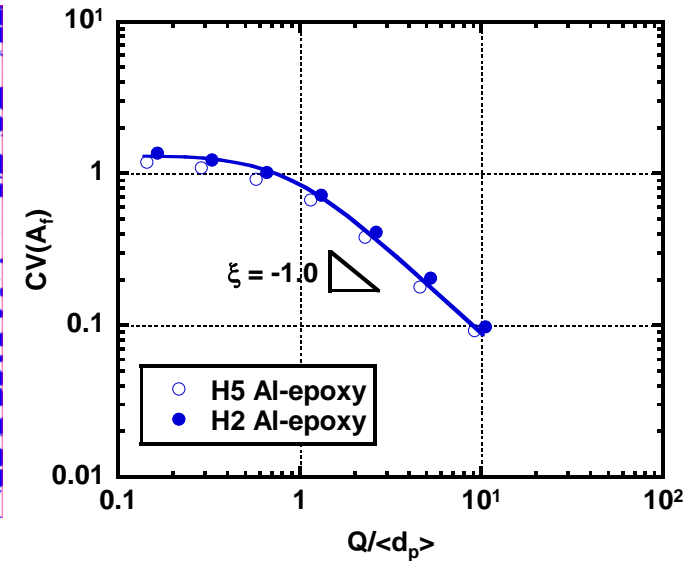
Cast-cure aluminum-epoxy composites made with two different grades of Al powder



Epoxy-65H5



Epoxy-65H2



- Both the H5 and H2 microstructures have similar spatial distributions
- Spatial distributions of Al in epoxy are statistically random, non-overlapping

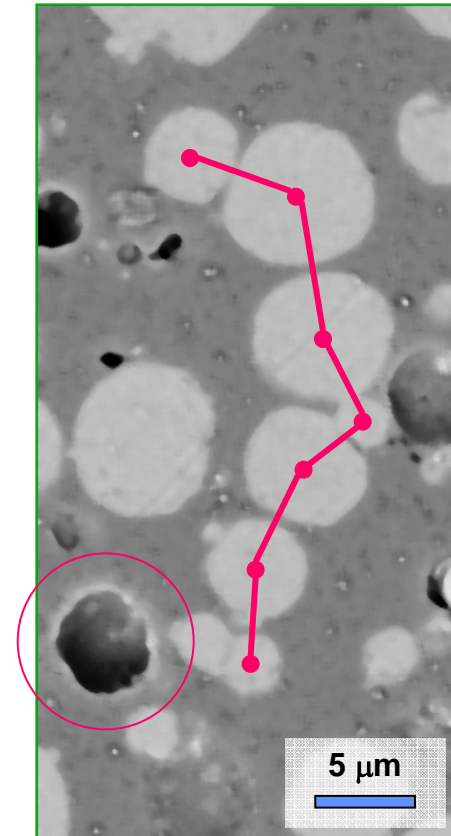
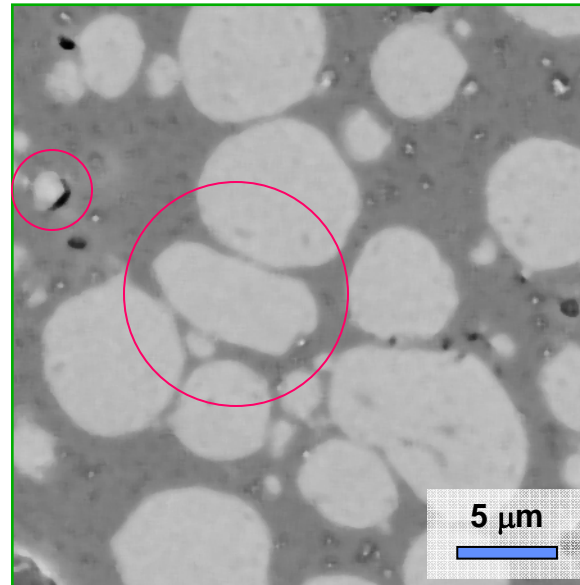
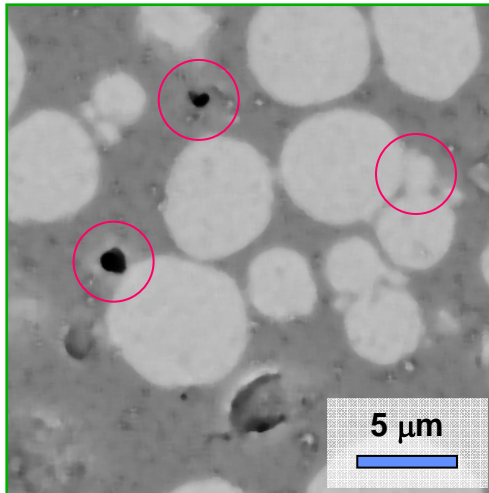
MSAAF allows quantification of mixing, phase distributions



Microstructural Details



Cast-cure aluminum-epoxy composite Epoxy-65H5



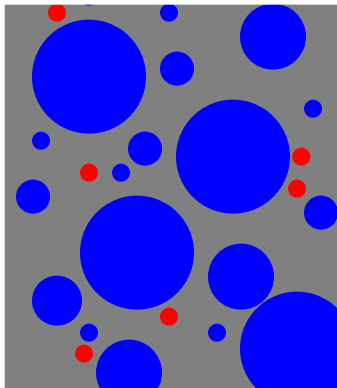
- Associated porosity
- Non-associated porosity
- Satellite particles
- Deformed particles
- Debonded particles
- Particle "chains"
- Pull-outs






Prediction of aluminum-epoxy mechanical properties



Hashin-Shtrikman (H-S) Bounds for Effective Elastic Modulus:



material		K (GPa)	G (GPa)	E (GPa)	ν (—)	f (—)
Aluminum		66.7	25.6	68.0	0.33	0.46
Epoxy		3.13	0.53	1.50	0.42	0.53
(porosity)		0.00	0.00	(—)	(—)	0.01

Bulk Modulus: $K_1^* < K^* < K_2^*$

Shear Modulus: $G_1^* < G^* < G_2^*$

Elastic Modulus (isotropic): $E_1^* = \frac{9K_1^*}{1 + 3K_1^*/G_1^*} ; E_2^* = \frac{9K_2^*}{1 + 3K_2^*/G_2^*}$



Prediction of aluminum-epoxy mechanical properties



H-S Bounds on K^ for 3-Phase System ($n=3$)*

material	K (GPa)	K_i
Aluminum	66.7	K_3
Epoxy	3.13	K_2
(pore)	0.00	K_1

$$K^*_1 = K_1 + \frac{A_1}{1 + \alpha_1 A_1}$$

$$K^*_2 = K_n + \frac{A_n}{1 + \alpha_n A_n}$$

$$\alpha_1 = -\frac{3}{3K_1 + 4G_1}$$

$$\alpha_n = -\frac{3}{3K_n + 4G_n}$$

$$A_1 = \sum_{i=2}^{i=n} \frac{f_i}{\frac{1}{K_i - K_1} - \alpha_1}$$

$$A_n = \sum_{i=1}^{i=n-1} \frac{f_i}{\frac{1}{K_i - K_n} - \alpha_n}$$

$$\boxed{K^*_1 < K^* < K^*_2}$$

$$\boxed{0.00 < K^* < 1.632 \text{ (GPa)}}$$



Prediction of aluminum-epoxy mechanical properties



H-S Bounds on G^ for 3-Phase System ($n=3$)*

material	G (GPa)	G_i
Aluminum	25.6	G_3
Epoxy	0.53	G_2
(pore)	0.00	G_1

$$G^*_1 = G_1 + \frac{B_1}{2(1 + \beta_1 B_1)}$$

$$G^*_2 = G_n + \frac{B_n}{2(1 + \beta_n B_n)}$$

$$\beta_1 = -\frac{3(K_1 + 2G_1)}{5G_1(3K_1 + 4G_1)}$$

$$\beta_n = -\frac{3(K_n + 2G_n)}{5G_n(3K_n + 4G_n)}$$

$$B_1 = \sum_{i=2}^{i=n} \frac{f_i}{\frac{1}{2(G_i - G_1)} - \beta_1}$$

$$B_n = \sum_{i=1}^{i=n-1} \frac{f_i}{\frac{1}{2(G_i - G_n)} - \beta_n}$$

$$\boxed{G^*_1 < G^* < G^*_2}$$

$$\boxed{0.00 < G^* < 0.279 \text{ (GPa)}}$$



Prediction of aluminum-epoxy mechanical properties



H-S Bounds on E^ for 3-Phase System ($n=3$)*

material	E (GPa)	f (—)
Aluminum	68.0	0.46
Epoxy	1.50	0.53
(pore)	(—)	0.01

$$E_1^* = \frac{9K_1^*}{1 + 3K_1^*/G_1^*} \quad ; \quad E_2^* = \frac{9K_2^*}{1 + 3K_2^*/G_2^*}$$

$$E_1^* < E^* < E_2^*$$

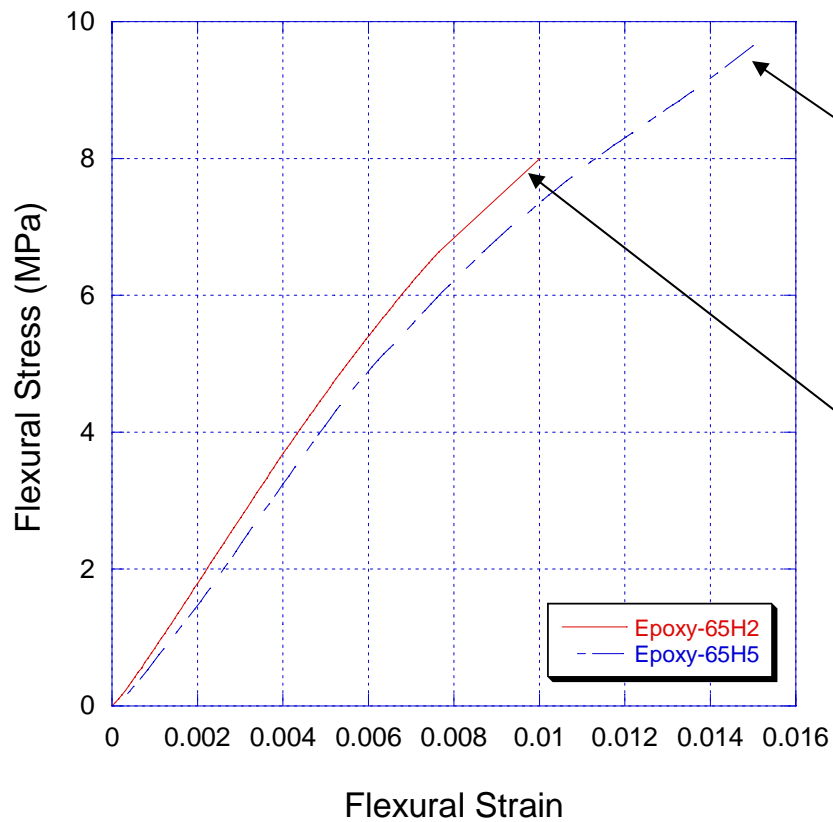
$$0.00 < E^* < 0.791 \text{ (GPa)}$$

- Model is very sensitive to exact porosity levels in each material.
- Model is very sensitive to large stiffness differences between phases.
- Model does not include influence of particle size.
- Only upper and lower bounds on elastic constants.
- Influence of microstructure is not explicitly addressed.

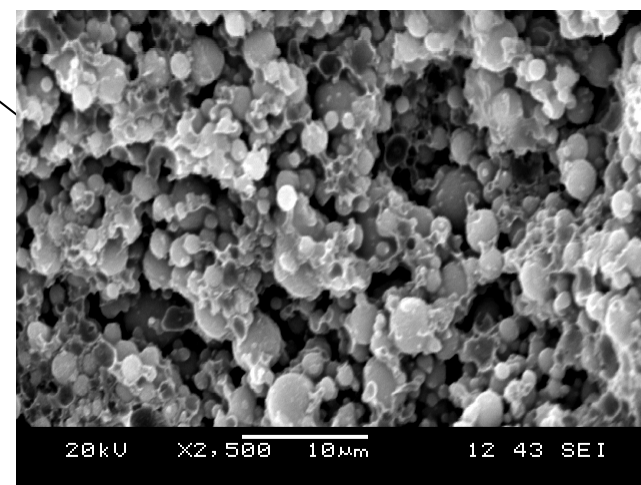
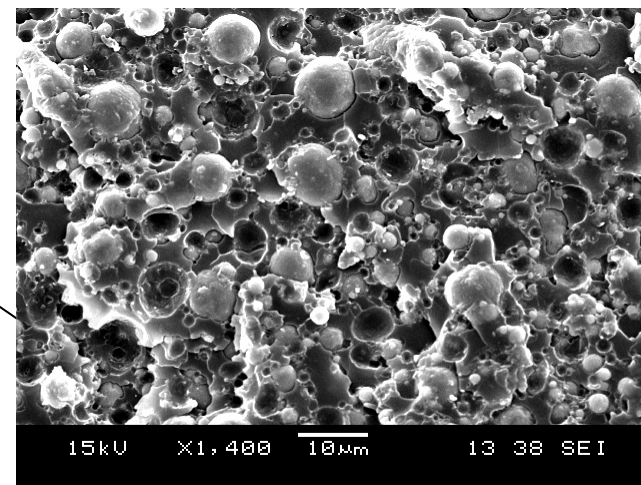
Microstructure-based modeling is needed



Flexural Testing



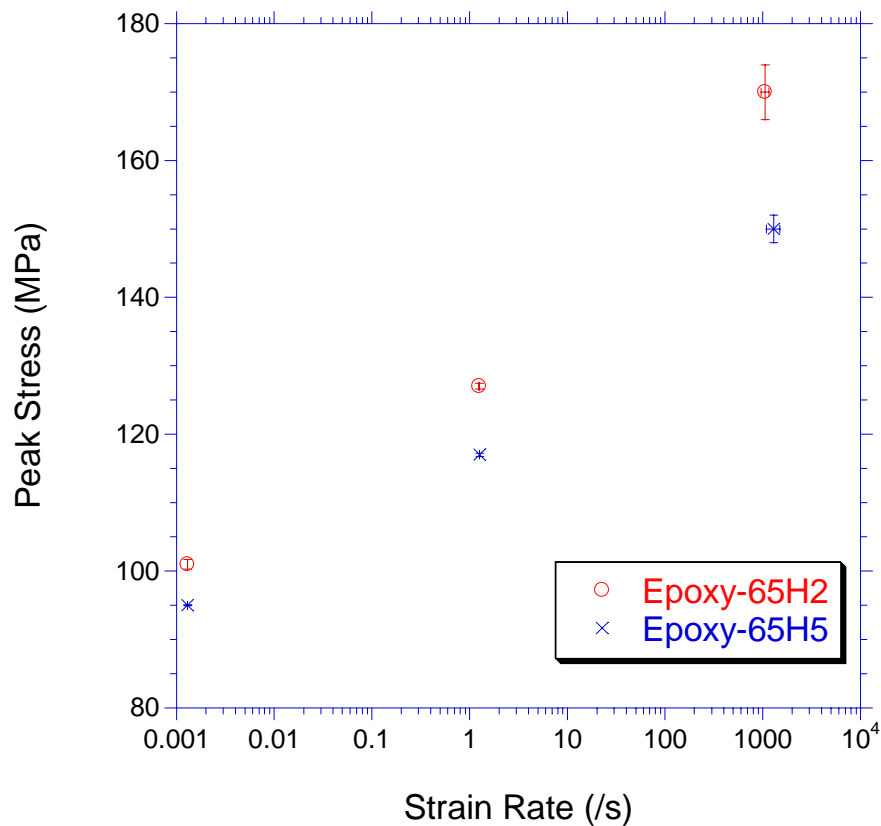
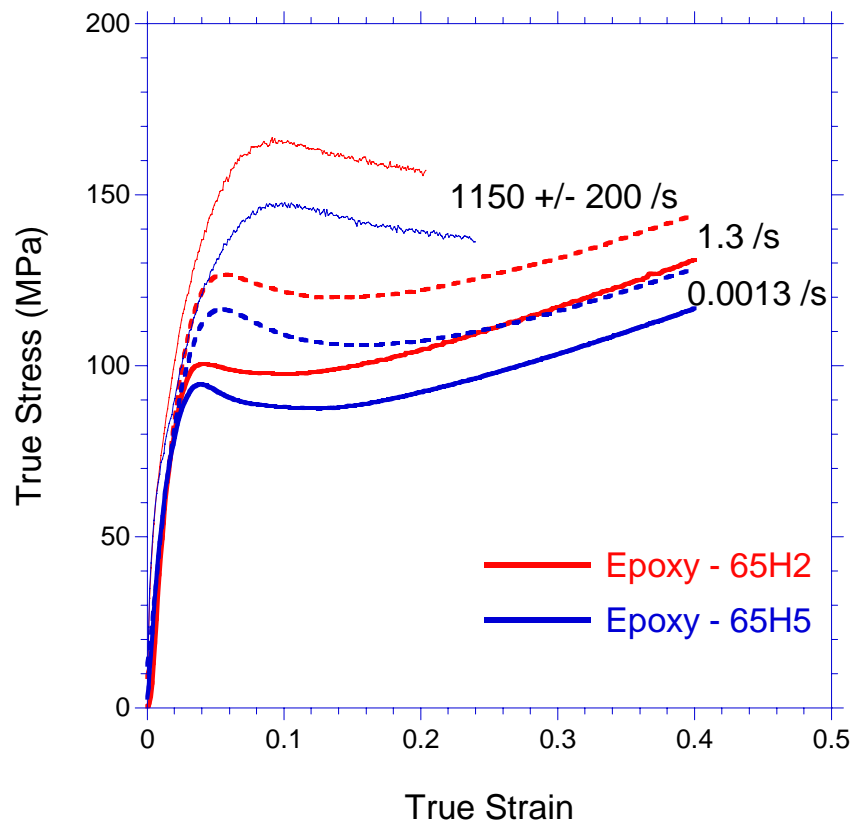
*Average of 5 experimental samples



Failure by particle pull-out



Compression Testing

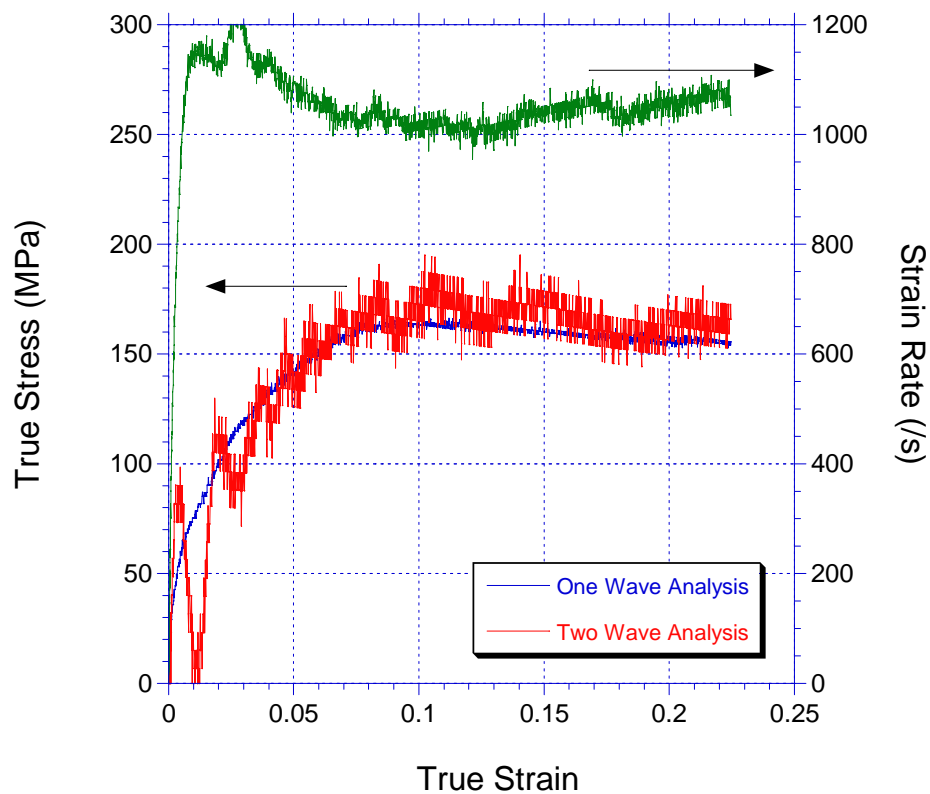




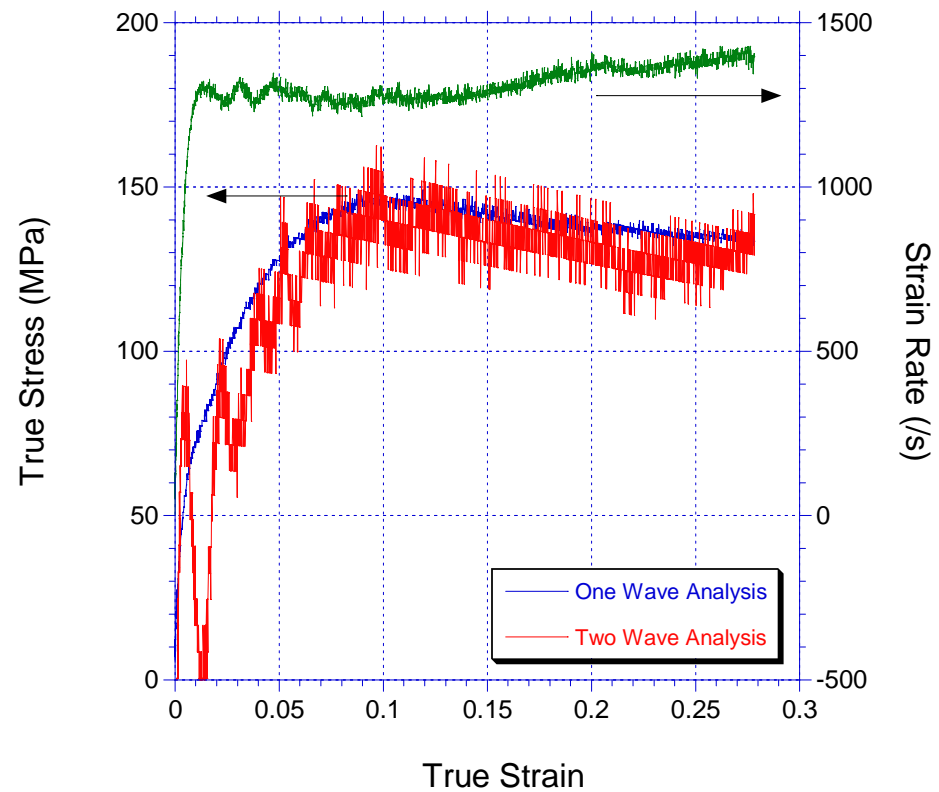
Stress Equilibrium



Epoxy – 65H2



Epoxy – 65H5





Aluminum-epoxy mechanical properties vs. particle size



Summary of Mechanical Test Data:

material	$\langle d_p \rangle$ (μm)	E (GPa)	σ_{fail} (MPa)	$\sigma_{\text{peak}} (\dot{\epsilon} = 10^{-3})$ (MPa)	$\sigma_{\text{peak}} (\dot{\epsilon} = 10^0)$ (MPa)	$\sigma_{\text{peak}} (\dot{\epsilon} = 10^3)$ (MPa)
Epoxy-65H2	3.5	0.92 ± 0.05	8.0 ± 0.8	101 ± 0.7	127 ± 0.4	170 ± 4
Epoxy-65H5	5.4	0.83 ± 0.03	9.6 ± 0.5	95 ± 0.1	117 ± 0.2	150 ± 2

Initial Guidance:

- Materials are extremely brittle in tension
- Lower flexural fail stress in H2 because more i/f per unit volume or weaker i/f
- Higher modulus in H5 potentially due to higher volume fraction
- Higher peak stress in H2 in compression due to larger number of particles per unit volume, constraint effects on epoxy flow behavior.
- **Difference between compression and tension reveals that the interface is relatively weak, compared with the strength of the epoxy matrix.**



Acknowledgements



- **Dr. Jay S. Tiley and Capt. Brett Conner, AFOSR program managers**
- **The authors would like to thank the MNM Model shop for sample preparation, particularly Mr. Frank Wise.**
- **Dr. Daniel B. Miracle, AFRL Nano-ST**